

# Nonreciprocal Quantum Entanglement Against Backscattering

Ya-Feng Jiao,<sup>1</sup> Sheng-Dian Zhang,<sup>1</sup> Yan-Lei Zhang,<sup>2,3</sup> Adam Miranowicz,<sup>4</sup> Le-Man Kuang,<sup>1,\*</sup> and Hui Jing<sup>1,†</sup>

<sup>1</sup>Key Laboratory of Low-Dimensional Quantum Structures and Quantum Control of Ministry of Education, Department of Physics and Synergetic Innovation Center for Quantum Effects and Applications, Hunan Normal University, Changsha 410081, China

<sup>2</sup>CAS Key Laboratory of Quantum Information, University of Science and Technology of China, Hefei 230026, P. R. China

<sup>3</sup>CAS Center For Excellence in Quantum Information and Quantum Physics, University of Science and Technology of China, Hefei, Anhui 230026, P. R. China

<sup>4</sup>Faculty of Physics, Adam Mickiewicz University, 61-614 Poznań, Poland

(Dated: November 25, 2021)

We propose how to achieve nonreciprocal light-sound entanglement in a spinning resonator and maintain its quality against backscattering losses. We find that by splitting the counter-propagating lights of the resonator via the Sagnac effect, quantum entanglement can be created from one side while prohibited from the other, and it is possible to switch such a single device between a classical isolator and a purely quantum diode. Particularly, in the presence of backscattering due to material imperfections in practical devices, significant entanglement revival can be achieved in a highly asymmetric way. This reveals a new strategy to protect quantum resources by engineering nonreciprocal devices, for building noise-tolerant quantum processors, realizing chiral networks, and invisible quantum sensing.

Unidirectional devices are indispensable in such diverse applications as chiral engineering, invisible sensing, and back-action-immune information processing [1]. By steering classical transmission rates, one-way light flow has been demonstrated by using atomic gases [2, 3], nonlinear devices [4–9], and moving media [10–12] or synthetic materials [13–16]. In view of advances of chiral quantum engineering [17–20], nonreciprocal control of quantum systems has also been pursued, such as single-photon diodes [21] or circulators [22], and one-way photon blockade [23–25]. However, as far as we know, the possibility of switching a single device between a classical isolator and a purely quantum diode, as well as protecting quantum resources against backscattering losses via nonreciprocity, has not yet been revealed.

In this work, we propose to achieve nonreciprocal quantum entanglement in cavity optomechanics (COM), revealing its unique properties which are otherwise unattainable in conventional reciprocal devices. We note that COM systems, based on radiation-pressure-induced light-motion coupling [26, 27], have provided powerful tools for quantum control of massive objects [28–33], achieving COM entanglement [34–41], and ultrasensitive metrology [42–44]. In a very recent work, quantum correlations at room temperature were demonstrated even between light and 40 kg mirrors [45]. Here, by combing quantum COM and nonreciprocal control, we show how to create one-way COM entanglement in a spinning resonator, and how to switch such a single device between a classical isolator and a purely quantum diode. Particularly, we find that for the same backscattering strength due to material imperfections, COM entanglement in a selected direction is significantly enhanced, in comparison with that in conventional devices. Our findings indicate a promising new way to protect fragile quantum resources by engineering nonreciprocal devices, which is useful in building noise-tolerant quantum processors [46, 47], realizing chiral quantum networks [17–20, 48], and invisible quantum sensing [49, 50].

As shown in Figs. 1(a) and 1(b), we consider a spinning resonator which is evanescently coupled with a tapered fiber. In a recent experiment [12], nonreciprocal propagation of light with 99.6 % isolation was demonstrated by using such a spinning device. Due to its rotation, the optical paths of counter-propagating lights in the resonator become different, which results in an irreversible effective refractive index for the clockwise (CW) and counter-clockwise (CCW) optical modes [12], i.e.,  $n_{\odot, \ominus} = n[1 \pm nR\Omega(n^{-2} - 1)/c]$ , where  $n$  is the refractive index of the material,  $\Omega$  is the angular velocity of the resonator with radius  $R$ , and  $c$  is the speed of light in the vacuum. Correspondingly, the resonance frequencies of the counter-propagating modes experience an opposite Sagnac-Fizeau shift [51], i.e.,  $\omega_c \rightarrow \omega_c + \Delta_F$  with

$$\Delta_F = \pm \Omega \frac{nR\omega_c}{c} \left( 1 - \frac{1}{n^2} - \frac{\lambda}{n} \frac{dn}{d\lambda} \right), \quad (1)$$

where  $\omega_c$  is the optical frequency of the stationary resonator, and the dispersion term  $dn/d\lambda$ , characterizing the relativistic origin of the Sagnac effect, is relatively small in typical materials (up to  $\sim 1\%$ ) [12]. Figure 1(c) shows the frequency spectrum of such a spinning COM system. For the resonator spinning along the CW direction, we have  $\Delta_F > 0$  or  $\Delta_F < 0$  for the case with the driven laser on the left or right hand side, and the effective optical frequency is  $\omega_j = \omega_c \pm |\Delta_F|$  ( $j = \odot, \ominus$ ), respectively. In addition, the resonator can support a mechanical breathing mode with frequency  $\omega_m$ . The Hamiltonian of this COM system, in a frame rotating with a driven frequency  $\omega_l$ , with the driven laser on the right-hand side, is ( $\hbar = 1$ ):

$$\begin{aligned} \hat{H} &= \hat{H}_c + \frac{\omega_m}{2} (\hat{p}^2 + \hat{q}^2) - G_0 (\hat{a}_{\odot}^{\dagger} \hat{a}_{\ominus} + \hat{a}_{\ominus}^{\dagger} \hat{a}_{\odot}) \hat{q}, \\ \hat{H}_c &= \sum_{j=\odot, \ominus} \Delta_j \hat{a}_j^{\dagger} \hat{a}_j + J (\hat{a}_{\odot}^{\dagger} \hat{a}_{\ominus} + \hat{a}_{\ominus}^{\dagger} \hat{a}_{\odot}) + i\varepsilon (\hat{a}_{\odot}^{\dagger} - \hat{a}_{\ominus}), \end{aligned} \quad (2)$$

where  $\hat{a}_j$  ( $\hat{a}_j^{\dagger}$ ) is the optical annihilation (creation) operator,

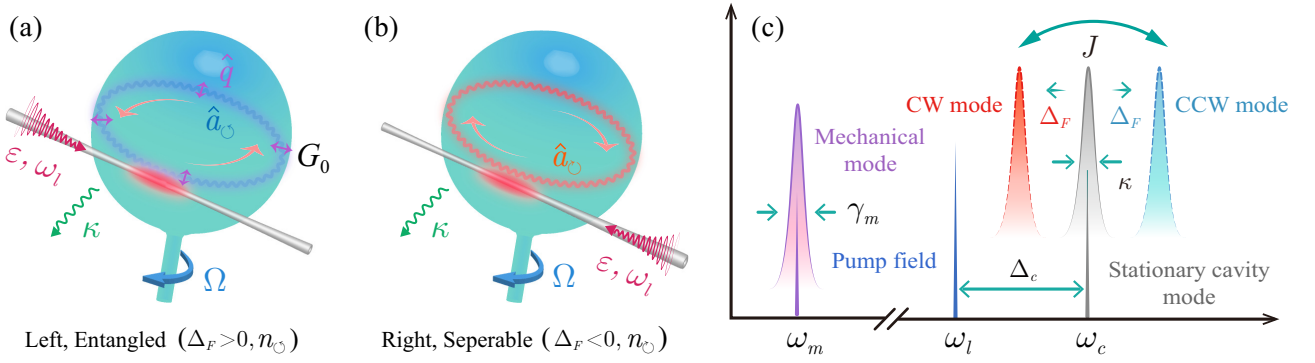


**Figure 1: Nonreciprocal optomechanical entanglement in a spinning resonator.** Since the counter-propagating lights in the spinning resonator experience opposite Sagnac-Fizeau frequency shifts, we have, by fixing the CW rotation of the resonator, (a)  $\Delta_F > 0$  for the case by driving the CCW mode, while (b)  $\Delta_F < 0$  for the case by driving the CW mode. For the same input light, by tuning the rotation velocity and optical detuning, COM entanglement can appear unidirectionally. (c) Frequency spectrum of the spinning COM system in (a) and (b). The mechanical mode is supported by radiation-pressure-induced radial breathing of the resonator. In terms of devices with inherent imperfections, the CW and CCW modes are coupled through backscattering with coupling strength  $J$ . See text for more details.

$\Delta_j = \omega_j - \omega_l$ , and  $\hat{q}(\hat{p})$  is the dimensionless mechanical displacement (momentum) operator. The field amplitude of the driving laser is  $|\varepsilon| = \sqrt{2\kappa P/\hbar\omega_l}$ , where  $P$  and  $\kappa$  are the input laser power and the optical decay rate, respectively. The optical coupling strength  $J$  denotes the backscattering process which is inevitable for practical materials with inherent imperfections,  $G_0 = (\omega_c/R)(m\omega_m)^{-1/2}$  is the single-photon COM coupling rate, with  $m$  denoting the mass of the resonator.

The quantum Langevin equations of this COM system then read:

$$\begin{aligned}\dot{\hat{a}}_\ominus &= -(i\Delta_\ominus + \kappa)\hat{a}_\ominus - iJ\hat{a}_\ominus + iG_0\hat{a}_\ominus\hat{q} + \sqrt{2\kappa}\hat{a}_\ominus^{\text{in}}, \\ \dot{\hat{a}}_\oplus &= -(i\Delta_\oplus + \kappa)\hat{a}_\oplus - iJ\hat{a}_\oplus + iG_0\hat{a}_\oplus\hat{q} + \varepsilon + \sqrt{2\kappa}\hat{a}_\oplus^{\text{in}}, \\ \dot{\hat{q}} &= \omega_m\hat{p}, \\ \dot{\hat{p}} &= -\omega_m\hat{q} - \gamma_m\hat{p} + G_0(\hat{a}_\oplus^\dagger\hat{a}_\ominus + \hat{a}_\ominus^\dagger\hat{a}_\oplus) + \hat{\xi},\end{aligned}\quad (3)$$

where  $\gamma_m$  is the mechanical damping rate, and  $\hat{a}_j^{\text{in}}(\hat{\xi})$  is the zero-mean input noise operator for the optical (mechanical) mode, characterized by the following correlation functions [52]:

$$\begin{aligned}\langle \hat{a}_j^{\text{in}}(t)\hat{a}_j^{\text{in},\dagger}(t') \rangle &= \delta(t-t'), \\ \langle \hat{\xi}(t)\hat{\xi}(t') \rangle &\simeq \gamma_m(2n_m + 1)\delta(t-t'), \text{ for } \omega_m/\gamma_m \gg 1,\end{aligned}\quad (4)$$

where  $n_m = [\exp(\hbar\omega_m/k_B T) - 1]^{-1}$  is the thermal phonon number,  $k_B$  is the Boltzmann constant, and  $T$  is the bath temperature. The zero-mean features of quantum noise can preserve the Gaussian nature of any initial state of the system [34]. By writing each operator as a sum of its steady-state mean value and a small fluctuation around it, i.e.,

$$\hat{a}_j = \alpha_j + \delta\hat{a}_j, \quad \hat{q} = q_s + \delta\hat{q}, \quad \hat{p} = p_s + \delta\hat{p}, \quad (5)$$

and defining the vectors of quadrature fluctuations and input noises as  $u^T(t) = (\delta\hat{X}_\ominus, \delta\hat{Y}_\ominus, \delta\hat{X}_\oplus, \delta\hat{Y}_\oplus, \delta\hat{q}, \delta\hat{p})$ ,  $v^T(t) =$

$(\sqrt{2\kappa}\hat{X}_\ominus^{\text{in}}, \sqrt{2\kappa}\hat{Y}_\ominus^{\text{in}}, \sqrt{2\kappa}\hat{X}_\oplus^{\text{in}}, \sqrt{2\kappa}\hat{Y}_\oplus^{\text{in}}, 0, \hat{\xi})$ , with the components:

$$\begin{aligned}\delta\hat{X}_j &= \frac{1}{\sqrt{2}}(\delta\hat{a}_j^\dagger + \delta\hat{a}_j), & \delta\hat{Y}_j &= \frac{i}{\sqrt{2}}(\delta\hat{a}_j^\dagger - \delta\hat{a}_j), \\ \hat{X}_j^{\text{in}} &= \frac{1}{\sqrt{2}}(\hat{a}_j^{\text{in}\dagger} + \hat{a}_j^{\text{in}}), & \hat{Y}_j^{\text{in}} &= \frac{i}{\sqrt{2}}(\hat{a}_j^{\text{in}\dagger} - \hat{a}_j^{\text{in}}),\end{aligned}\quad (6)$$

we can obtain a compact form of the linearized equations of fluctuations

$$\dot{u}(t) = Au(t) + v(t), \quad (7)$$

where

$$A = \begin{pmatrix} -\kappa & \tilde{\Delta}_\ominus & 0 & J & -G_\ominus^y & 0 \\ -\tilde{\Delta}_\ominus & -\kappa & -J & 0 & G_\ominus^x & 0 \\ 0 & J & -\kappa & \tilde{\Delta}_\oplus & -G_\oplus^y & 0 \\ -J & 0 & -\tilde{\Delta}_\oplus & -\kappa & G_\oplus^x & 0 \\ 0 & 0 & 0 & 0 & 0 & \omega_m \\ G_\oplus^x & G_\oplus^y & G_\ominus^x & G_\ominus^y & -\omega_m & -\gamma_m \end{pmatrix}, \quad (8)$$

and  $\tilde{\Delta}_j = \Delta_j - G_0q_s$  is the effective optical detuning,  $G_j^x$  ( $G_j^y$ ) is the real (imaginary) part of the effective COM coupling rate:  $G_j \equiv \sqrt{2}G_0\alpha_j = G_j^x + iG_j^y$ , and the steady-state solutions of the dynamical variables are given by:

$$\begin{aligned}\alpha_\ominus &= \frac{-iJ\varepsilon}{(i\tilde{\Delta}_\ominus + \kappa)(i\tilde{\Delta}_\ominus + \kappa) + J^2}, \\ \alpha_\oplus &= \frac{-\tilde{\Delta}_\ominus + i\kappa}{J}\alpha_\ominus, \\ q_s &= \frac{G_0}{\omega_m}(|\alpha_\oplus|^2 + |\alpha_\ominus|^2), \quad p_s = 0.\end{aligned}\quad (9)$$

The solution of the fluctuations in Eq. (7) is given by  $u(t) = \mathcal{M}(t)u(0) + \int_0^t d\tau \mathcal{M}(t-\tau)v(\tau)$ , where  $\mathcal{M}(t) = \exp(At)$ . The system is stable when all the real parts of the

eigenvalues of  $A$  are negative, as characterized by the Routh-Hurwitz criterion [53]. Under this stability condition, we have  $\mathcal{M}(\infty) = 0$  in the steady state and

$$u_i(\infty) = \int_0^\infty d\tau \sum_k \mathcal{M}_{ik}(\tau) v_k(t - \tau). \quad (10)$$

This COM system finally evolves into a Gaussian state, which is fully characterized by a  $6 \times 6$  correlation matrix  $V$ , with its components

$$V_{kl} = \langle u_k(\infty) u_l(\infty) + u_l(\infty) u_k(\infty) \rangle / 2. \quad (11)$$

Using Eqs. (4) and (10), the steady-state correlation matrix  $V$  is obtained as

$$V = \int_0^\infty d\tau \mathcal{M}(\tau) D \mathcal{M}^T(\tau), \quad (12)$$

where  $D = \text{Diag}[\kappa, \kappa, \kappa, \kappa, 0, \gamma_m(2n_m + 1)]$  is a diagonal matrix characterizing the stationary noise correlations. When the stability condition is satisfied, Eq. (12) is determined by the Lyapunov equation [34]

$$AV + VA^T = -D. \quad (13)$$

By solving this linear Eq. (13), we can calculate quantum correlations of the fluctuations and also the logarithmic negativity,  $E_{\mathcal{N}}$ , as a bipartite entanglement measure of continuous variables, i.e., [54]

$$E_{\mathcal{N}} = \max[0, -\ln(2\nu^-)], \quad (14)$$

with

$$\nu^- = \frac{1}{\sqrt{2}} \left\{ \mathcal{F}(\mathcal{V}_{bp}) - \left[ \mathcal{F}(\mathcal{V}_{bp})^2 - 4 \det \mathcal{V}_{bp} \right]^{1/2} \right\}^{1/2}, \quad (15)$$

and  $\mathcal{F}(\mathcal{V}_{bp}) = \det \mathcal{A} + \det \mathcal{B} - 2 \det \mathcal{C}$ . Here  $\nu^-$  is the lowest symplectic eigenvalue of the partial transpose of a bipartite  $4 \times 4$  correlation matrix,  $\mathcal{V}_{bp}$ , which is obtained by selecting the rows and columns of the interesting modes in  $V$  and has a  $2 \times 2$  block form

$$\mathcal{V}_{bp} = \begin{pmatrix} \mathcal{A} & \mathcal{C} \\ \mathcal{C}^T & \mathcal{B} \end{pmatrix}. \quad (16)$$

We see from Eq. (14) that COM entanglement can be achieved only for  $\nu^- < 1/2$ .

In our numerical calculations, for ensuring the system staying in the stable regime, we use the following experimentally feasible parameters [12, 55]:  $n = 1.48$ ,  $m = 10$  ng,  $R = 1.1$  mm,  $\lambda = 1.55$   $\mu\text{m}$ ,  $Q = \omega_c/\kappa = 3.2 \times 10^7$ ,  $\omega_m = 63$  MHz,  $\gamma_m = 5.2$  kHz,  $T = 130$  mK, and  $\Omega = 8$  kHz or 23 kHz. We first consider the ideal case without optical backscattering, i.e.,  $J = 0$ , and we plot the logarithmic negativity  $E_{\mathcal{N}}$  and the intracavity photon number  $N_j$  in Fig. 2 as a function of the optical detuning  $\Delta_c = \omega_c - \omega_l$ . For a stationary resonator,

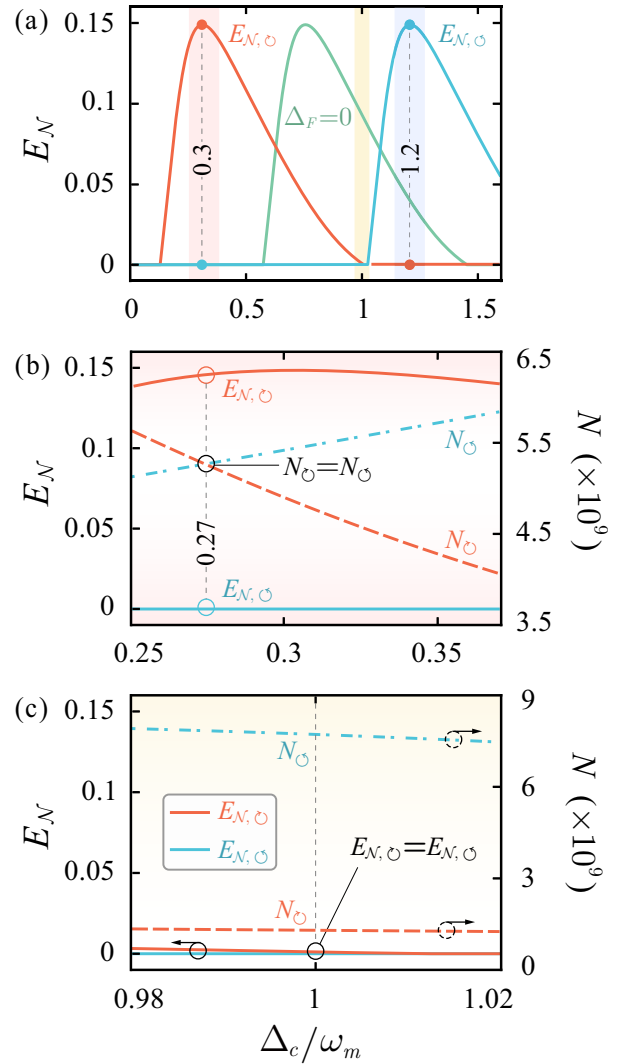


**Figure 2: Nonreciprocal photon-phonon entanglement without backscattering.** (a) The logarithmic negativity  $E_{\mathcal{N}}$  versus the scaled optical detuning  $\Delta_c/\omega_m$  for different input directions. For the non-spinning case with  $\Delta_F = 0$ , COM entanglement does not rely on the input directions and always appears around the resonance  $\Delta_c/\omega_m \simeq 1$  (gray dotted curve). In the presence of rotation, nonreciprocal entanglement emerges around  $\Delta_c/\omega_m = 0.3$  or 1.2, i.e., COM entanglement is created or prohibited for the opposite input direction. (b-c) Tunable quantum nonreciprocity versus classical nonreciprocity. For  $\Delta_c/\omega_m \sim 0.27$ , quantum nonreciprocity exists even when  $N_{\circ} = N_{\ominus}$  (i.e., no classical nonreciprocity); in contrast to this, for  $\Delta_c/\omega_m \sim 1$ , classical nonreciprocity can appear for  $E_{\mathcal{N}, \circ} = E_{\mathcal{N}, \ominus}$ . The parameters are chosen as  $\Omega = 8$  kHz,  $J = 0$ , and  $P = 20$  mW. See text for details of the other parameters.

$E_{\mathcal{N}}$  remains the same independently of driving it from the left or right hand side; in contrast, for a spinning resonator,  $E_{\mathcal{N}}$  can be significantly different by reversing the driving direction. For example, as shown in Figs. 2(a) and 2(b), when the maximal COM entanglement is generated by driving the setup from one side, i.e.,  $E_{\mathcal{N}} \sim 0.15$ , no entanglement occurs by driving it from the other side, i.e.,  $E_{\mathcal{N}} \sim 0$ . This is a clear

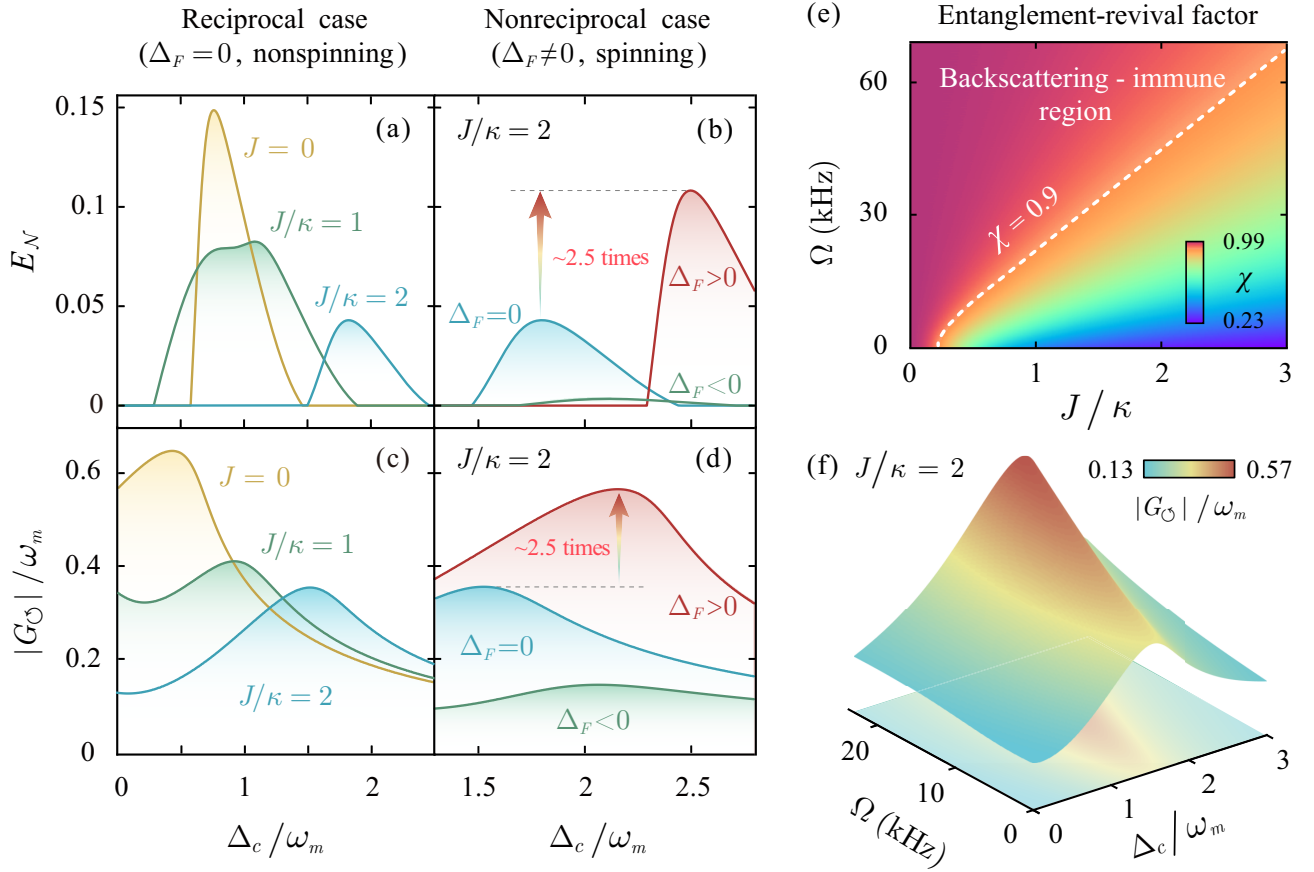


**Figure 3: Suppression of COM entanglement due to random-defect-induced backscattering, and its nonreciprocal revival resulting from the rotation-induced compensation.** (a,b) The logarithmic negativity  $E_N$  and (c,d) the effective COM coupling  $G_\odot/\omega_m$  are plotted as a function of the scaled optical detuning  $\Delta_c/\omega_m$ . For  $\Omega = 23$  kHz, the value of  $E_N$  is enhanced for  $\sim 2.5$  times, reaching almost that as in an ideal device without backscattering. (e) Density plot of the revival factor  $\chi$  as a function of the optical coupling strength  $J$  and the rotation speed  $\Omega$ . (f) The effective COM coupling  $G_\odot/\omega_m$  versus the optical detuning  $\Delta_c/\omega_m$  and the rotation speed  $\Omega$ .

signature of quantum nonreciprocity, which is fundamentally different from that in classical devices showing only nonreciprocal transmission rates. In fact, as shown in Figs. 2(b) and 2(c), for  $\Delta_c/\omega_m \sim 0.27$ , nonreciprocal COM entanglement exists even when there is no classical nonreciprocity (i.e.,  $N_\odot = N_\ominus$ ); in contrast, for  $\Delta_c/\omega_m \sim 1$ , significant classical nonreciprocity can appear for  $E_{N,\odot} \simeq E_{N,\ominus}$ . This difference between classical and quantum nonreciprocities can be easily understood by the fact that the COM entanglement is created by the Stokes or anti-Stokes scattering process between the mechanical mode and the driving field. These results indicate that it is possible to switch a single device between a classical isolator and a purely quantum diode.

More importantly, we find that nonreciprocal quantum control provides a feasible way to overcome various harmful effects of nonideal factors such as surface roughness or material inhomogeneity in a practical device. As Fig. 3 shows, in a conventional COM system, for  $J \neq 0$ ,  $E_N$  always decreases. In comparison, nonreciprocal entanglement can be more robust, which is reminiscent of the defect-insensitive entanglement in topological structures or chiral environment [18, 19].

For example, for  $J/\kappa = 2$ , the maximum value of  $E_N$  in a spinning resonator can be enhanced by a factor of 2.5, approaching to that in an ideal resonator [see Fig. 3(b)]. To better understand this counterintuitive effect, we further plot the effective COM coupling  $|G_\odot|$  with respect to the optical detuning in Figs. 3(c), 3(d) and 3(f). We see that in a conventional COM system, larger values of  $J$  always lead to the suppression of the effective coupling and, thus, the decreasing of  $E_N$ . However, in a spinning device, the backscattering-induced reflection can be significantly suppressed. Hence, as a result, an almost ideal COM entanglement can be achieved due to the enhanced effective COM coupling, which can be clearly demonstrated by defining a factor of entanglement revival:

$$\chi = \frac{\max[E_N(\Omega \neq 0, J \neq 0)]}{\max[E_N(\Omega = 0, J = 0)]}. \quad (17)$$

As shown in Fig. 3(e), the maximal revival factor  $\chi$  can reach a value even up to 99.1%, indicating that COM entanglement can be made immune to backscattering losses in a nonreciprocal way. This may serve as a promising new method to improve the performance of quantum devices against inher-

ent imperfections by harnessing the power of nonreciprocal devices. Also we have confirmed that nonreciprocal entanglement can survive even when the COM entanglement is fully destroyed by thermal noises in a conventional reciprocal device (see supplementary information for details).

Finally, we remark that quantum COM entanglement has been demonstrated in various systems [36–41]. In these experiments, to verify the created entanglement, one needs to measure the corresponding correlation matrix  $\mathcal{V}_{bp}$ , which requires to access all the quadrature fluctuations in the optical and mechanical canonical variables [36–38]. Specifically, the optical quadrature fluctuations can be measured straightforwardly through a homodyne or heterodyne detection of the output field. While by applying a weak probe laser to the COM resonator at the red-sideband frequency  $\omega_p = \omega_c - \omega_m$ , the mechanical motion can be mapped to the sidebands of the probe at the cavity resonance [36, 40]. Using this well-established procedure for the output of the spinning resonator, one can also verify the nonreciprocal features of COM entanglement.

In summary, we have shown that quantum photon-phonon entanglement, a key element in quantum COM devices, can be created in a highly asymmetric way. Such nonreciprocal entanglement turns out to be robust against random backscattering losses, without the use of any complicated topological design or dissipation engineering. Our work opens up a range of exciting opportunities for quantum information processing, networking and metrology by exploiting the power of quantum nonreciprocity. The ability to manipulate quantum states or nonclassical correlations in a nonreciprocal way sheds new lights on chiral quantum engineering and can stimulate more works on achieving and operating quantum nonreciprocal devices, such as directional quantum squeezing [30, 31], backaction-immune quantum sensing [56, 57], and quantum chiral coupling of COM devices to superconducting qubits or atomic spins [58–64].

We thank Chang-Ling Zou for helpful discussions. L.-M. K. is supported by the National Natural Science Foundation of China (NSFC, 11775075 and 11434011). H. J. is supported by the NSFC (11474087, 11774086, 11935006). A. M. is supported by the Polish National Science Centre (NCN) under the Maestro Grant No. DEC-2019/34/A/ST2/00081. Y.-L. Z. is supported by the NSFC (11704370).

\* Electronic address: [lmkuang@hunnu.edu.cn](mailto:lmkuang@hunnu.edu.cn)

† Electronic address: [jinghui73@gmail.com](mailto:jinghui73@gmail.com)

- [1] Y. Shoji and T. Mizumoto, Magneto-optical non-reciprocal devices in silicon photonics, *Sci. Technol. Adv. Mater.* **15**, 014602 (2014).
- [2] H. Ramezani, P. K. Jha, Y. Wang, and X. Zhang, Nonreciprocal Localization of Photons, *Phys. Rev. Lett.* **120**, 043901 (2018).
- [3] S. Zhang, Y. Hu, G. Lin, Y. Niu, K. Xia, J. Gong, and S. Gong, Thermal-motion-induced non-reciprocal quantum optical system, *Nat. Photonics* **12**, 744 (2018).
- [4] S. Manipatruni, J. T. Robinson, and M. Lipson, Optical Nonreciprocity in Optomechanical Structures, *Phys. Rev. Lett.* **102**, 213903 (2009).
- [5] Z. Shen, Y.-L. Zhang, Y. Chen, C.-L. Zou, Y.-F. Xiao, X.-B. Zou, F.-W. Sun, G.-C. Guo, and C.-H. Dong, Experimental realization of optomechanically induced non-reciprocity, *Nat. Photonics* **10**, 657 (2016).
- [6] N. R. Bernier, L. D. Tóth, A. Koottandavida, M. A. Ioannou, D. Malz, A. Nunnenkamp, A. K. Feofanov, and T. J. Kippenberg, Nonreciprocal reconfigurable microwave optomechanical circuit, *Nat. Commun.* **8**, 604 (2017).
- [7] L. M. de Lépinay, E. Damskägg, C. F. Ockeloen-Korppi, and M. A. Sillanpää, Realization of Directional Amplification in a Microwave Optomechanical Device, *Phys. Rev. Appl.* **11**, 034027 (2019).
- [8] C.-H. Dong, Z. Shen, C.-L. Zou, Y.-L. Zhang, W. Fu, and G.-C. Guo, Brillouin-scattering-induced transparency and nonreciprocal light storage, *Nat. Commun.* **6**, 6193 (2015).
- [9] X.-W. Xu, Y. Li, B. Li, H. Jing, and A.-X. Chen, Nonreciprocity via Nonlinearity and Synthetic Magnetism, *Phys. Rev. Appl.* **13**, 044070 (2020).
- [10] D.-W. Wang, H.-T. Zhou, M.-J. Guo, J.-X. Zhang, J. Evers, and S.-Y. Zhu, Optical Diode Made from a Moving Photonic Crystal, *Phys. Rev. Lett.* **110**, 093901 (2013).
- [11] Y. Yang, C. Peng, D. Zhu, H. Buljan, J. D. Joannopoulos, B. Zhen, and M. Soljačić, Synthesis and observation of non-Abelian gauge fields in real space, *Science* **365**, 1021 (2019).
- [12] S. Maayani, R. Dahan, Y. Kligerman, E. Moses, A. U. Hassan, H. Jing, F. Nori, D. N. Christodoulides, and T. Carmon, Flying couplers above spinning resonators generate irreversible refraction, *Nature (London)* **558**, 569 (2018).
- [13] D. L. Sounas and A. Alù, Non-reciprocal photonics based on time modulation, *Nat. Photonics* **11**, 774 (2017).
- [14] B. Peng, Ş. K. Özdemir, F. Lei, F. Monifi, M. Gianfreda, G. L. Long, S. Fan, F. Nori, C. M. Bender, and L. Yang, Parity-time-symmetric whispering-gallery microcavities, *Nat. Phys.* **10**, 394 (2014).
- [15] B. Peng, Ş. K. Özdemir, M. Liertzer, W. Chen, J. Kramer, H. Yilmaz, J. Wiersig, S. Rotter, and L. Yang, Chiral modes and directional lasing at exceptional points, *Proc. Natl. Acad. Sci. U. S. A.* **113**, 6845 (2016).
- [16] Q. Zhong, S. Nelson, Ş. K. Özdemir, and R. El-Ganainy, Controlling directional absorption with chiral exceptional surfaces, *Opt. Lett.* **44**, 5242 (2019).
- [17] P. Lodahl, S. Mahmoodian, S. Stobbe, A. Rauschenbeutel, P. Schneeweiss, J. Volz, H. Pichler, and P. Zoller, Chiral quantum optics, *Nature (London)* **541**, 473 (2017).
- [18] C. Gonzalez-Ballester, A. Gonzalez-Tudela, F. J. Garcia-Vidal, and E. Moreno, Chiral route to spontaneous entanglement generation, *Phys. Rev. B* **92**, 155304 (2015).
- [19] S. A. H. Gangaraj, G. W. Hanson, and M. Antezza, Robust entanglement with three-dimensional nonreciprocal photonic topological insulators, *Phys. Rev. A* **95**, 063807 (2017).
- [20] G. Hu, X. Hong, K. Wang, *et al.*, Coherent steering of nonlinear chiral valley photons with a synthetic Au-WS<sub>2</sub> metasurface, *Nat. Photonics* **13**, 467 (2019).
- [21] K. Xia, F. Nori, and M. Xiao, Cavity-Free Optical Isolators and Circulators Using a Chiral Cross-Kerr Nonlinearity, *Phys. Rev. Lett.* **121**, 203602 (2018).
- [22] M. Scheucher, A. Hilico, E. Will, J. Volz, and A. Rauschenbeutel, Quantum optical circulator controlled by a single chirally coupled atom, *Science* **354**, 1577 (2016).
- [23] R. Huang, A. Miranowicz, J.-Q. Liao, F. Nori, and H. Jing, Nonreciprocal Photon Blockade, *Phys. Rev. Lett.* **121**, 153601 (2018).

- (2018).
- [24] B. Li, R. Huang, X. Xu, A. Miranowicz, and H. Jing, Nonreciprocal unconventional photon blockade in a spinning optomechanical system, *Photon. Res.* **7**, 630 (2019).
- [25] P. Yang, M. Li, X. Han, H. He, G. Li, C.-L. Zou, P. Zhang, and T. Zhang, Non-reciprocal cavity polariton, [arXiv:1911.10300](https://arxiv.org/abs/1911.10300).
- [26] M. Aspelmeyer, T. J. Kippenberg, and F. Marquardt, Cavity optomechanics, *Rev. Mod. Phys.* **86**, 1391 (2014).
- [27] E. Verhagen, S. Deléglise, S. Weis, A. Schliesser, and T. J. Kippenberg, Quantum-coherent coupling of a mechanical oscillator to an optical cavity mode, *Nature (London)* **482**, 63 (2012).
- [28] S. Hong, R. Riedinger, I. Marinković, A. Wallucks, S. G. Hofer, R. A. Norte, M. Aspelmeyer, and S. Gröblacher, Hanbury Brown and Twiss interferometry of single phonons from an optomechanical resonator, *Science* **358**, 203 (2017).
- [29] F. Lecocq, J. B. Clark, R. W. Simmonds, J. Aumentado, and J. D. Teufel, Quantum Nondemolition Measurement of a Non-classical State of a Massive Object, *Phys. Rev. X* **5**, 041037 (2015).
- [30] E. E. Wollman, C. U. Lei, A. J. Weinstein, J. Suh, A. Kronwald, F. Marquardt, A. A. Clerk, and K. C. Schwab, Quantum squeezing of motion in a mechanical resonator, *Science* **349**, 952 (2015).
- [31] J.-M. Pirkkalainen, E. Damskägg, M. Brandt, F. Massel, and M. A. Sillanpää, Squeezing of Quantum Noise of Motion in a Micromechanical Resonator, *Phys. Rev. Lett.* **115**, 243601 (2015).
- [32] K. Stannigel, P. Rabl, A. S. Sørensen, P. Zoller, and M. D. Lukin, Optomechanical Transducers for Long-Distance Quantum Communication, *Phys. Rev. Lett.* **105**, 220501 (2010).
- [33] M. Mirhosseini, A. Sipahigil, M. Kalaei, and O. Painter, Quantum transduction of optical photons from a superconducting qubit, [arXiv:2004.04838](https://arxiv.org/abs/2004.04838).
- [34] D. Vitali, S. Gigan, A. Ferreira, H. R. Böhm, P. Tombesi, A. Guerreiro, V. Vedral, A. Zeilinger, and M. Aspelmeyer, Optomechanical Entanglement between a Movable Mirror and a Cavity Field, *Phys. Rev. Lett.* **98**, 030405 (2007).
- [35] S. Huang and G. S. Agarwal, Entangling nanomechanical oscillators in a ring cavity by feeding squeezed light, *New J. Phys.* **11**, 103044 (2009).
- [36] T. A. Palomaki, J. D. Teufel, R. W. Simmonds, and K. W. Lehnert, Entangling Mechanical Motion with Microwave Fields, *Science* **342**, 710 (2013).
- [37] S. Barzanjeh, E. S. Redchenko, M. Peruzzo, M. Wulf, D. P. Lewis, G. Arnold, and J. M. Fink, Stationary entangled radiation from micromechanical motion, *Nature (London)* **570**, 480 (2019).
- [38] J. Chen, M. Rossi, D. Mason, and A. Schliesser, Entanglement of propagating optical modes via a mechanical interface, *Nat. Commun.* **11**, 943 (2020).
- [39] R. Riedinger, S. Hong, R. A. Norte, J. A. Slater, J. Shang, A. G. Krause, V. Anant, M. Aspelmeyer, and S. Gröblacher, Non-classical correlations between single photons and phonons from a mechanical oscillator, *Nature (London)* **530**, 313 (2016).
- [40] C. F. Ockeloen-Korppi, E. Damskägg, J.-M. Pirkkalainen, M. Asjad, A. A. Clerk, F. Massel, M. J. Woolley, and M. A. Sillanpää, Stabilized entanglement of massive mechanical oscillators, *Nature (London)* **556**, 478 (2018).
- [41] R. Riedinger, A. Wallucks, I. Marinković, C. Löschnauer, M. Aspelmeyer, S. Hong, and S. Gröblacher, Remote quantum entanglement between two micromechanical oscillators, *Nature (London)* **556**, 473 (2018).
- [42] F. Massel, S. U. Cho, J.-M. Pirkkalainen, P. J. Hakonen, T. T. Heikkilä, and M. A. Sillanpää, Multimode circuit optomechanics near the quantum limit, *Nat. Commun.* **3**, 987 (2012).
- [43] D. E. McClelland, N. Mavalvala, Y. Chen, and R. Schnabel, Advanced interferometry, quantum optics and optomechanics in gravitational wave detectors, *Laser Photon. Rev.* **5**, 677 (2011).
- [44] S. Qvarfort, A. Serafini, P. F. Barker, and S. Bose, Gravimetry through non-linear optomechanics, *Nat. Commun.* **9**, 3690 (2018).
- [45] H. Yu *et al.*, Quantum correlations between the light and kilogram-mass mirrors of LIGO, [arXiv:2002.01519](https://arxiv.org/abs/2002.01519).
- [46] K. Stannigel, P. Komar, S. J. M. Habraken, S. D. Bennett, M. D. Lukin, P. Zoller, and P. Rabl, Optomechanical Quantum Information Processing with Photons and Phonons, *Phys. Rev. Lett.* **109**, 013603 (2012).
- [47] R. Horodecki, P. Horodecki, M. Horodecki, and K. Horodecki, Quantum entanglement, *Rev. Mod. Phys.* **81**, 865 (2009).
- [48] H. J. Kimble, The quantum internet, *Nature (London)* **453**, 1023 (2008).
- [49] R. Fleury, D. Sounas, and A. Alù, An invisible acoustic sensor based on parity-time symmetry, *Nat. Commun.* **6**, 5905 (2015).
- [50] T. Yang, X. Bai, D. Gao, L. Wu, B. Li, J. T. L. Thong, and C.-W. Qiu, Invisible Sensors: Simultaneous Sensing and Camouflaging in Multiphysical Fields, *Adv. Mater.* **27**, 7752 (2015).
- [51] G. B. Malykin, The Sagnac effect: correct and incorrect explanations, *Phys. Usp.* **43**, 1229 (2000).
- [52] C. W. Gardiner and P. Zoller, *Quantum Noise* (Springer, Berlin, 2000).
- [53] E. X. DeJesus and C. Kaufman, Routh-Hurwitz criterion in the examination of eigenvalues of a system of nonlinear ordinary differential equations, *Phys. Rev. A* **35**, 5288 (1987).
- [54] G. Adesso, A. Serafini, and F. Illuminati, Extremal entanglement and mixedness in continuous variable systems, *Phys. Rev. A* **70**, 022318 (2004).
- [55] G. C. Righini, Y. Dumeige, P. Féron, M. Ferrari, G. N. Conti, D. Ristic, and S. Soria, Whispering gallery mode microresonators: Fundamentals and applications, *Riv. Nuovo Cimento* **34**, 435 (2011).
- [56] F. Wolfgramm, C. Vitelli, F. A. Beduini, N. Godbout, and M. W. Mitchell, Entanglement-enhanced probing of a delicate material system, *Nat. Photonics* **7**, 28 (2013).
- [57] Y. Ma, H. Miao, B. H. Pang, M. H. Evans, C. Zhao, J. Harms, R. Schnabel, and Y. Chen, Proposal for gravitational-wave detection beyond the standard quantum limit through EPR entanglement, *Nat. Phys.* **13**, 776 (2017).
- [58] L. DiCarlo, M. D. Reed, L. Sun, B. R. Johnson, J. M. Chow, J. M. Gambetta, L. Frunzio, S. M. Girvin, M. H. Devoret, and R. J. Schoelkopf, Preparation and measurement of three-qubit entanglement in a superconducting circuit, *Nature (London)* **467**, 574 (2010).
- [59] C. F. Ockeloen-Korppi, E. Damskägg, G. S. Paraoanu, F. Massel, and M. A. Sillanpää, Revealing Hidden Quantum Correlations in an Electromechanical Measurement, *Phys. Rev. Lett.* **121**, 243601 (2018).
- [60] P. Kurpiers, P. Magnard, T. Walter, B. Royer, M. Pechal, J. Heinsoo, Y. Salathé, A. Akin, S. Storz, J.-C. Besse, S. Gasparinetti, A. Blais, and A. Wallraff, Deterministic quantum state transfer and remote entanglement using microwave photons, *Nature (London)* **558**, 264 (2018).
- [61] J. Li, S.-Y. Zhu, and G. S. Agarwal, Magnon-Photon-Phonon Entanglement in Cavity Magnomechanics, *Phys. Rev. Lett.* **121**, 203601 (2018).
- [62] X.-Y. Lü, G.-L. Zhu, L.-L. Zheng, and Y. Wu, Entanglement and quantum superposition induced by a single photon, *Phys. Rev. A* **97**, 033807 (2018).
- [63] W. Qin, A. Miranowicz, P.-B. Li, X.-Y. Lü, J. Q. You, and

- F. Nori, Exponentially Enhanced Light-Matter Interaction, Cooperativities, and Steady-State Entanglement Using Parametric Amplification, *Phys. Rev. Lett.* **120**, 093601 (2018).
- [64] T. M. Karg, B. Gouraud, C. T. Ngai, G.-L. Schmid, K. Hammerer, and P. Treutlein, Light-mediated strong coupling between a mechanical oscillator and atomic spins 1 meter apart, *Science* [10.1126/science.abb0328](https://doi.org/10.1126/science.abb0328) (2020).

## Supplementary Information for “Nonreciprocal Quantum Entanglement Against Backscattering”

Ya-Feng Jiao,<sup>1</sup> Sheng-Dian Zhang,<sup>1</sup> Yan-Lei Zhang,<sup>2,3</sup> Adam Miranowicz,<sup>4</sup> Le-Man Kuang,<sup>1,\*</sup> and Hui Jing<sup>1,†</sup>

<sup>1</sup>*Key Laboratory of Low-Dimensional Quantum Structures and Quantum Control of Ministry of Education,  
Department of Physics and Synergetic Innovation Center for Quantum Effects and Applications,  
Hunan Normal University, Changsha 410081, China*

<sup>2</sup>*CAS Key Laboratory of Quantum Information, University of Science and Technology of China, Hefei 230026, P. R. China*

<sup>3</sup>*CAS Center For Excellence in Quantum Information and Quantum Physics, University of Science and Technology of China,  
Hefei, Anhui 230026, P. R. China*

<sup>4</sup>*Faculty of Physics, Adam Mickiewicz University, 61-614 Poznań, Poland*

Here, we present the technical details on nonreciprocal photon-phonon entanglement. Our discussion includes: (1) experimental feasibility of our proposed scheme, including the stable coupling of the tapered fiber and the spinning resonator; (2) stability analysis, including the mechanical and optical stability; (3) backscattering-induced suppression and nonreciprocal revival of photon-phonon entanglement; (4) other quantum nonreciprocity, including nonreciprocal entanglement dimensionality and unidirectional cross-quadrature two-mode squeezing; (5) thermal effect on nonreciprocal entanglement.

### Contents

<b>References</b>	<b>5</b>
<b>S1. Experimental feasibility</b>	<b>2</b>
A. Self-adjustment process	2
B. Intermolecular forces	3
<b>S2. Stability conditions</b>	<b>4</b>
A. Mechanical stability	4
B. Optical stability	4
<b>S3. Nonreciprocal control and backscattering process</b>	<b>6</b>
<b>S4. Entanglement dimensionality and two mode squeezing</b>	<b>7</b>
<b>S5. Influence of thermal effect on optomechanical entanglement</b>	<b>8</b>
<b>S6. System parameters</b>	<b>9</b>
<b>References</b>	<b>9</b>

## S1. EXPERIMENTAL FEASIBILITY

### A. Self-adjustment process

Our realization of the quantum nonreciprocity requires that the counter-propagating modes experience an opposite Sagnac-Fizeau frequency shift. Inspired by a recent experiment [S1], our approach is to use a spinning microsphere resonator, which is mounted on a turbine and spins with the stability of its axis. In their experimental setup, the silica microsphere with radius  $r = 1.1$  mm is positioned near a single-mode telecommunication fiber, and thus light can be coupled into or out of the resonator evanescently. The angular velocity of the resonator can reach a value of  $\Omega = 6.6$  kHz. Moreover, by using levitated nanomechanical rotors, the values of  $\Omega$  can be further improved, reaching even up to the GHz regime [S2, S3].

For such spinning devices [S1], the aerodynamic process plays a key role in the stable fiber-resonator coupling. Specifically, the fast spinning resonator can drag air into the region between the tapered fiber and the resonator, thereby forming a lubrication layer of air in this region. Then the thin film of air, exerting pressure on the surface of the tapered fiber facing the resonator, can make the fiber fly above the resonator with the separation of a few nanometres. Besides, if any perturbation causes the taper to rise higher than the stable-equilibrium height, it can float back to its original position, which is referred to as “self-adjustment” behavior. In this condition, the separation of the fiber from a spinning resonator can be enabled—that is, the fiber will not touch or stick to the resonator even if it is pushed towards the spinning microsphere [S1], which is in contrast to the situation for a stationary resonator (i.e., the taper may stick to the microsphere due to the van der Waals forces).

To give further explain the “self-adjustment” behavior, we perform a force analysis of the local deformation of the tapered fiber in the following. By breaking the fiber into a series of infinitesimal cylinders, the air pressure, which leads to a displacement  $d$  of the outermost one, can be written as  $\Delta T_{\text{air}} = (\rho\Delta\theta)T_{\text{air}}/L$ , with  $\rho$  ( $\theta$ ) the radius (angle) of the winding shape of the deformation region. Then, the total air pressure  $T_{\text{air}}$  on the taper can be estimated analytically as [S1]

$$T_{\text{air}} = 6.19\mu R^{5/2}\Omega \int_0^r \left(h - \sqrt{r^2 - x^2} + r\right)^{-3/2} dx, \quad (\text{S1.1})$$

where  $\mu$  is the viscosity of air,  $R$  ( $r$ ) is the radius of the microsphere (taper), and  $h = h_0 + d$  represents the taper-resonator separation, with  $h_0$  denoting the stationary gap between the fiber and the sphere.

Meanwhile, the local deformation will also lead to a tension on the infinitesimal cylinder, which can be calculated by

$$\Delta T_{\text{ela}} = 2\mathcal{F} \sin(\Delta\theta/2) \approx \mathcal{F}\Delta\theta, \quad (\text{S1.2})$$

where  $\mathcal{F}$  is the elastic force on the taper that obeys the Hooke law:  $\sigma = \epsilon E$ . The parameter  $\sigma = \mathcal{F}/(\pi r^2)$  is the uniaxial stress,  $E$  is the Young modulus of silica, and  $\epsilon = \delta_L/L$  is the strain, where  $\delta_L = L' - L$  denotes the variation of the original length  $L$  of the deformation region. Furthermore,  $\delta_L$  can be straightforwardly derived via the following relations:  $L' = \rho\theta$ ,  $(L/2)^2 + (\rho - d)^2 = \rho^2$ , and  $\sin(\theta/2) = L/(2\rho)$ . Hence, in the case of equilibrium (i.e.,  $\Delta T_{\text{air}} = \Delta T_{\text{ela}}$ ),  $T_{\text{air}}$  can be given in another form:

$$T_{\text{air}} = 2\pi r^2 E [\arcsin(\phi) - \phi] \approx \frac{\pi}{3} r^2 \phi^3 E, \quad (\text{S1.3})$$

where  $\phi = 4Ld/(L^2 + 4d^2)$ , and the approximation,  $\arcsin(\phi) = \phi + \phi^3/6 + \dots$ , is made within the limit of  $|\phi| \ll 1$ , which physically requires a comparatively small distortion. As shown in Fig. S1(a), we confirmed that these approximation conditions can be easily satisfied with experimentally accessible parameters [S1, S4]:  $E = 75$  GPa,  $r = 544$  nm, and  $L = 3$   $\mu\text{m}$ . In this case, the displacement  $d$  can be analytically described as

$$d = \frac{L}{2} \left(\beta - \sqrt{\beta^2 - 1}\right), \quad (\text{S1.4})$$

where  $\beta = [\pi r^2 E / (3T_{\text{air}})]^{1/3}$ . Therefore, the strain of the taper can be reduced to  $\epsilon = \arcsin(\phi)/\phi - 1 \approx \phi^2/6$ . From this expression, we find that the strain (i.e., the elastic force) is positively associated with the taper-resonator separation:

$$\frac{\partial \mathcal{F}}{\partial h} = \pi r^2 E \left(\frac{\partial \epsilon}{\partial d}\right) = \frac{16\pi r^2 E L^2 d (L^2 - 4d^2)}{3(L^2 + 4d^2)^3} > 0. \quad (\text{S1.5})$$

Equation (S1.5) clearly reveals that the elastic force becomes stronger when the air gap gets larger than the stable-equilibrium distance. Meanwhile, as shown in Fig. S1(b), the air pressure on the taper is notably suppressed. As a result, the taper can be dragged back to its original position when any perturbation causes it far away from the spinning resonator, leading to the self-adjustment behavior. The self-adjustment of the tapered fiber enables the critical coupling of light into or out of the resonator, by which the counter-propagating beams can experience an optical drag identical in size, but opposite in sign.

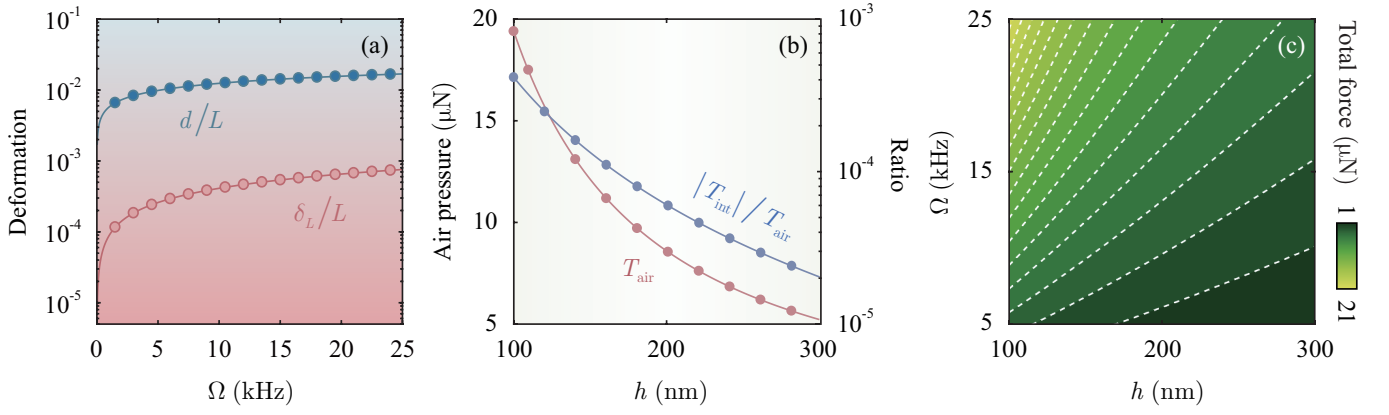


**Figure S1: Analysis of the “self-adjustment” behavior.** (a) The strain  $\epsilon$  and the displacement  $d$  as a function of the angular velocity  $\Omega$  for  $h = 250$  nm. (b) The air pressure  $T_{\text{air}}$  and the ratio of intermolecular forces  $|T_{\text{int}}|/T_{\text{air}}$  for varying taper-resonator separation  $h$  at  $\Omega = 23$  kHz. (c) Total force between the fiber and the sphere versus angular velocity  $\Omega$  and separation  $h$ . The resulting force of air pressure and intermolecular forces has a minimal value of  $T_{\text{tot}} = 1.135 \mu\text{N}$ , which indicates the interactions of the fiber and the spinning sphere are always repulsive.

### B. Intermolecular forces

The intermolecular forces in our device, such as the Casimir and van der Waals forces, can be described as [S1]:

$$T_{\text{int}} = rR \left( -\frac{\mathbb{A}}{6\pi h^3} + \frac{\mathbb{B}}{45\pi h^9} - \frac{\pi^2 c \hbar}{240 h^4} \right), \quad (\text{S1.6})$$

where the Hamaker constant  $\mathbb{A}$  can be calculated by [S5]:

$$\mathbb{A} = \frac{3\varepsilon_-^{(1)}\varepsilon_-^{(2)}k_{\text{B}}\text{T}}{4\varepsilon_+^{(1)}\varepsilon_+^{(2)}} + \frac{\nu \left[ n_-^{(1)}n_-^{(2)} \right]^2}{n_+^{(1)}n_+^{(2)} \left[ n_+^{(1)} + n_+^{(2)} \right]}, \quad (\text{S1.7})$$

with  $\nu = 3\sqrt{2}\hbar\nu_e/16$ ,  $\varepsilon_{\pm}^{(u)} = \varepsilon_u \pm \varepsilon_0$ ,  $n_{\pm}^{(u)} = \sqrt{n_u^2 \pm n_0^2}$ , and  $u = 1, 2$ . Hereafter, we use  $\varepsilon_0$  ( $n_0$ ),  $\varepsilon_1$  ( $n_1$ ), and  $\varepsilon_2$  ( $n_2$ ) to represent the dielectric constant (the refractive index) of air, the taper and the spinning resonator, respectively;  $k_{\text{B}}$  is the Boltzmann constant,  $\text{T}$  is the mechanical bath temperature, and  $\nu_e = 3$  PHz [S5]. Note that for simplicity, we have replaced  $n_2$  with  $n$  in the main text. Moreover, the constant  $\mathbb{B}$  is typically of the order of  $10^{-76}$  J m<sup>6</sup> for interactions between condensed matter phases across the vacuum or air [S6]. Taking intermolecular forces into account, the total force between the taper and the resonator becomes:  $T_{\text{tot}} = T_{\text{air}} + T_{\text{int}}$ . Herein, we choose experimentally accessible parameters [S7]:  $\varepsilon_0 = 1$ ,  $\varepsilon_1 = \varepsilon_2 = 3.9$ ,  $n_0 = 1$ ,  $n_1 = n_2 = 1.48$ , and  $\text{T} = 130$  mK. As expected, the intermolecular forces are found to be negligible ( $< 0.1\%$ ), and the taper-resonator interactions remain repulsive [see Figs. S1(b) and S1(c)]. Thus, the effects of the Casimir and van der Waals forces can be safely omitted on critical coupling.

In addition, the microsphere resonator is required to be perfectly spherical to maintain a stable evanescent coupling at high angular velocities. However, standard experimental methods for realizing whispering-gallery-mode microresonators are so mature that the silica spheres can be fabricated with almost atomically small surface roughness and nearly perfect shape via surface tension or polishing techniques. Hence, the influence of the sphere shape and the inherent backscattering are almost negligible for the stability of taper-resonator coupling. Other factors, such as lubricant compressibility, tapered-fiber stiffness, and the wrap angle of a fiber, may also affect critical coupling. However, these factors are confirmed to be negligible in experiments, which can be also safely ignored in our discussions [S1].

## S2. STABILITY CONDITIONS

### A. Mechanical stability

The condition of  $\tau \geq 1$  in Eq. (S1.4) yields the first limit of angular velocity:

$$\Omega_0 = \frac{\varrho\pi r^2 E}{18.57\mu R^{5/2}}, \quad (\text{S2.8})$$

where

$$\varrho = \left[ \int_0^r \left( h - \sqrt{r^2 - x^2} + r \right)^{-3/2} dx \right]^{-1}. \quad (\text{S2.9})$$

Also, the tiny displacement obeys  $d = h - h_0 < h$ , so that gives another limit:

$$\Omega_1 = \frac{\varrho\pi r^2 \Lambda E}{18.57\mu R^{5/2}}, \quad (\text{S2.10})$$

where  $\Lambda = [4Lh/(L^2 + 4h^2)]^3$ . Finally, the elastic limit of the taper provides the third condition ( $\sigma = \Upsilon$ ):

$$\Omega_2 = \frac{\varrho\pi r^2 \Upsilon}{3.095\mu R^{5/2}} \sqrt{\frac{6\Upsilon}{E}}, \quad (\text{S2.11})$$

where  $\Upsilon$  is typically 9 GPa for silica [S8]. Thus, the mechanical limit of the angular velocity can be given by:

$$\Omega_{\max} = \min \{ \Omega_0, \Omega_1, \Omega_2 \}. \quad (\text{S2.12})$$

When operating at taper-resonator separations near 250 nm, we find  $\Omega_0 = 81.6$  MHz,  $\Omega_1 = 2.8$  MHz,  $\Omega_2 = 49.9$  MHz, and  $\Omega_{\max} = 2.8$  MHz. Therefore, it is reasonable to set  $\Omega = 8$  kHz or 23 kHz in the main text. We have also checked the validity of the Taylor expansion in Eq. (S1.3):

$$\Pi = \arcsin(\phi) - \phi - \phi^3/6 < 9.11 \times 10^{-8}, \quad (\text{S2.13})$$

which proves the validity of our approximations.

Moreover, the radial displacement of the breathing mode may also affect the stable coupling of the fiber and the rotating sphere. For this reason, we compare the mean mechanical displacement  $x_s$  with the air-induced displacement  $d$ , given by

$$\eta = x_s/d = q_s x_{zp}/d, \quad (\text{S2.14})$$

where  $x_{zp} = \sqrt{\hbar/(m\omega_m)}$  denotes the standard deviation of the zero-point motion of the mechanical mode. As shown in Fig. S2(a), the effect of the mechanical displacement is negligible indeed ( $< 1\%$ ), thereby the radial breathing of the resonator does not disturb the critical evanescent coupling. Note that, for simplicity, we have introduced  $\Omega_r = \pm\Omega$ .

### B. Optical stability

According to the Routh-Hurwitz criterion [S9], the system is stable and reaches its steady state when all eigenvalues of the matrix  $A$  have negative real parts. Therefore, we start our analysis by determining the eigenvalues of the matrix  $A$ , i.e.,  $|A - \lambda I| = 0$ , which yields the characteristic equation:

$$\lambda^6 + a_1\lambda^5 + a_2\lambda^4 + a_3\lambda^3 + a_4\lambda^2 + a_5\lambda + a_6 = 0, \quad (\text{S2.15})$$

where

$$\begin{aligned} a_1 &= 4\kappa + \gamma_m, & a_2 &= \sigma_0 + \omega_m^2 + 4\kappa(\kappa + \gamma_m), \\ a_3 &= \sigma_0(2\kappa + \gamma_m) + 4\kappa(\omega_m^2 + \kappa\gamma_m), & a_4 &= \sigma_0\sigma_1 + \sigma_2 + 4\kappa^2\omega_m^2, \\ a_5 &= \gamma_m\mu_2 - 2\kappa\mu_0\mu_3(\gamma_m\mu_0 + 4\kappa\omega_m^2) + \kappa\mu_1(\kappa\gamma_m + 2\omega_m^2), \\ a_6 &= \omega_m(\sigma_+ + \sigma_- + \sigma_2\omega_m - \mu_0\mu_4) - \mu_3\tilde{\Delta}_+\tilde{\Delta}_-, \end{aligned}$$

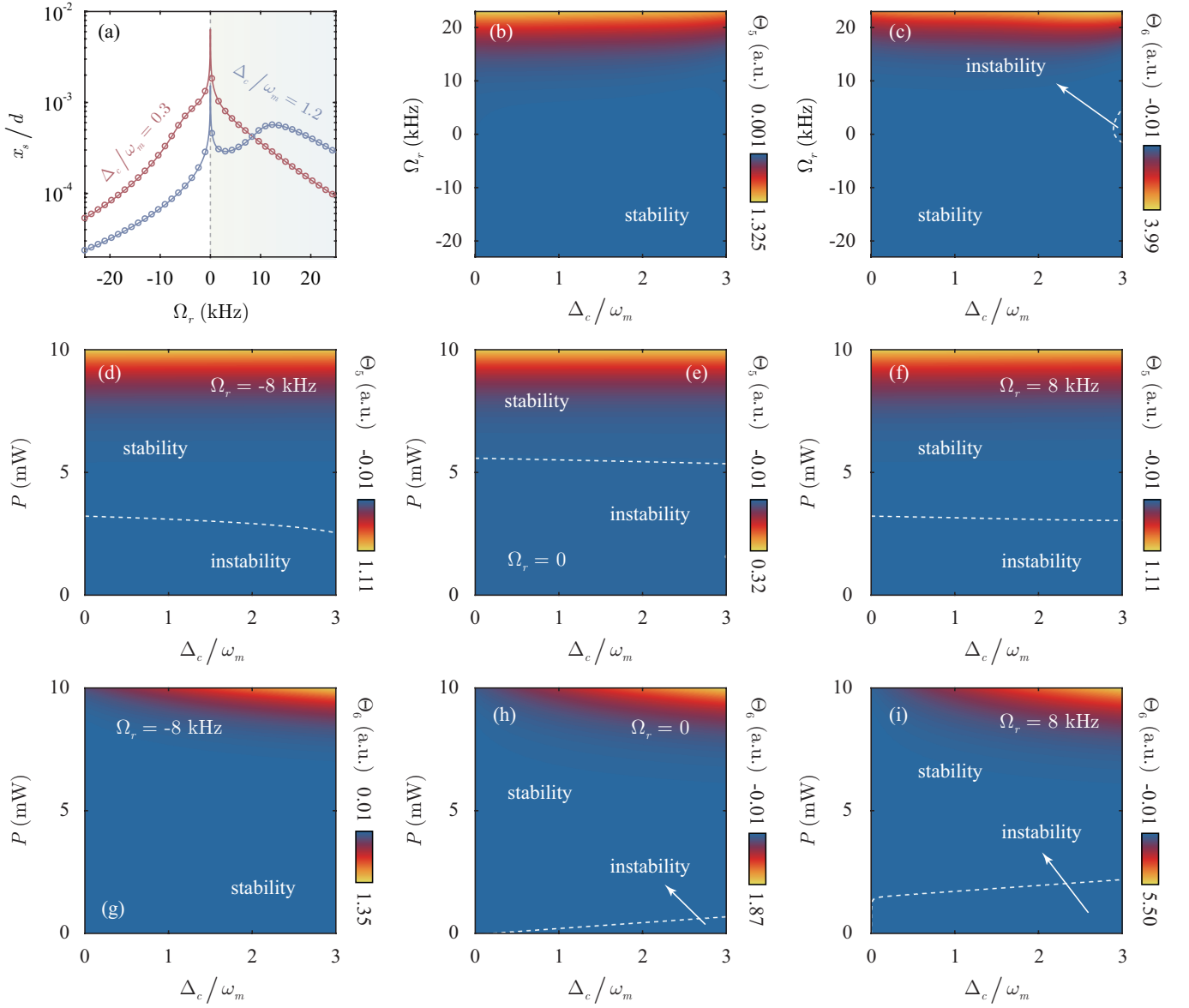


**Figure S2: The mechanical and optical stability conditions.** (a) The ratio of the mean mechanical displacement  $x_s$  to the air-induced displacement  $d$  as a function of the angular velocity  $\Omega_r$ . In the aerodynamic process, this ratio is extremely small ( $\sim 0.1\%$ ), meaning that radial breathing of the resonator is negligible compared to the air-induced displacement. (b-c) Stability functions  $\Theta_5$  and  $\Theta_6$  versus the angular velocity  $\Omega_r$  and the scaled optical detuning  $\Delta_c/\omega_m$  at  $J/\kappa = 2$  and  $P = 20$  mW. (d-i) Stability functions  $\Theta_5$  and  $\Theta_6$  versus the input power  $P$  and the scaled optical detuning  $\Delta_c/\omega_m$  at  $J = 0$  for different driving directions. White contour lines correspond to  $\Theta_5 = 0$  or  $\Theta_6 = 0$ , and a.u. represents arbitrary units. Other parameters are listed in Table I.

$$\begin{aligned}
\sigma_0 &= 2\mu_0 + \mu_1, & \sigma_1 &= \kappa^2 + 2\kappa\gamma_m + \omega_m^2, & \sigma_2 &= \mu_0^2 + \kappa^2\mu_1 + \mu_2, \\
\sigma_2 &= \mu_2 - \mu_3 + \mu_0(J^2 - \kappa^2), & \sigma_{\pm} &= (\Delta_{\pm}J^2 - \Delta_{\mp}\kappa^2)G_{\mp}^2, \\
\mu_0 &= J^2 + \kappa^2, & \mu_1 &= \tilde{\Delta}_+^2 + \tilde{\Delta}_-^2, & \mu_2 &= (\tilde{\Delta}_+\tilde{\Delta}_- - 2J^2)\tilde{\Delta}_+\tilde{\Delta}_-, \\
\mu_3 &= \omega_m(\tilde{\Delta}_+|G_{\odot}|^2 + \tilde{\Delta}_-|G_{\odot}|^2 + \mu_4), & \mu_4 &= 2J(G_{\odot}^x G_{\odot}^x + G_{\odot}^y G_{\odot}^y).
\end{aligned} \tag{S2.16}$$

Using the coefficients  $a_k$ , we can form a set of  $k \times k$  matrices,  $M_k$ , for  $k \leq 6$ , with their entries defined as:

$$M_{ln} = \begin{cases} 0, & 2l - n < 0 \text{ or } 2l - n > k, \\ a_{2l-n}, & \text{otherwise.} \end{cases} \tag{S2.17}$$

Then the stability condition can be satisfied by ensuring the determinants of all the matrix  $M_k$  are positive. For this reason, we

define the stability functions  $\Theta_s$  ( $s = 1, 2, \dots, 6$ ) as follows:

$$\begin{aligned}\Theta_1 &= a_1, \quad \Theta_2 = a_1 a_2 - a_3, \quad \Theta_3 = a_1 a_2 a_3 + a_1 a_5 - a_1^2 a_4 - a_3^2, \\ \Theta_4 &= a_1 a_2 a_3 a_4 + a_2 a_6 (a_1^2 + a_3) + a_1 a_5 (a_4 + a_5) - a_1^2 a_4^2 - a_1 a_3 a_6 - a_3^2 a_4 - a_4^2, \\ \Theta_5 &= a_1 a_2 a_3 a_4 a_5 + a_5 a_6 (a_1^2 a_2 - a_2 a_3 + a_1 a_3) + a_5^2 (a_2 a_3 + a_1 a_4 - a_1 a_2^2 - a_5) - a_3^2 (a_1 a_2 a_6 + a_4 a_5), \\ \Theta_6 &= a_1 a_2 a_3 a_4 a_5 a_6 + a_5 a_6 (a_1 a_4^2 - a_1^2 a_4^2 - a_3^2 a_4) + a_2 a_3 a_5^2 a_6 - a_1 a_2 a_3^2 a_6^2 - a_1 a_3 a_5 a_6^2 - a_5^3 a_6,\end{aligned}\quad (\text{S2.18})$$

whose signs decide if the system is stable:

$$\text{sgn}(\Theta_s) = \begin{cases} 1, & \text{implies stability,} \\ \text{otherwise,} & \text{implies instability.} \end{cases}\quad (\text{S2.19})$$

As shown in Figs. S2(b)-S2(i), we numerically plot the functions  $\Theta_5$  and  $\Theta_6$  to present the boundary between the stability and the instability regions. Moreover, we note that the other functions are always positive within the parameters we have used in the main text, such that these functions are not needed to be reported here. From the analysis made above, we can conclude that the spinning COM system remains stable in our numerical simulations.

### S3. NONRECIPROCAL CONTROL AND BACKSCATTERING PROCESS

In the main text, we have performed detailed comparisons of classical and quantum nonreciprocity. Here, for a better clarification of classical nonreciprocity, we plot the intracavity photon number  $N_j$  as a function of the optical detuning in Fig. S3(a). Apparently, the CW and CCW modes are reciprocal for the nonspinning case—that is, the intracavity photon number remains the same regardless of the driving directions. However, in the presence of rotation, the flow of light in the counter-propagating modes becomes asymmetric and the maximal isolation appears at the resonance  $\hat{\Delta}_j = \Delta_j - G_0 q_s = 0$ , indicating that the optical isolation is due to the change of the resonance condition caused by the Sagnac effect. It should be noted that such a kind of optical isolation is corresponding to classical nonreciprocity, since it only reveals the direction-dependent control of particle

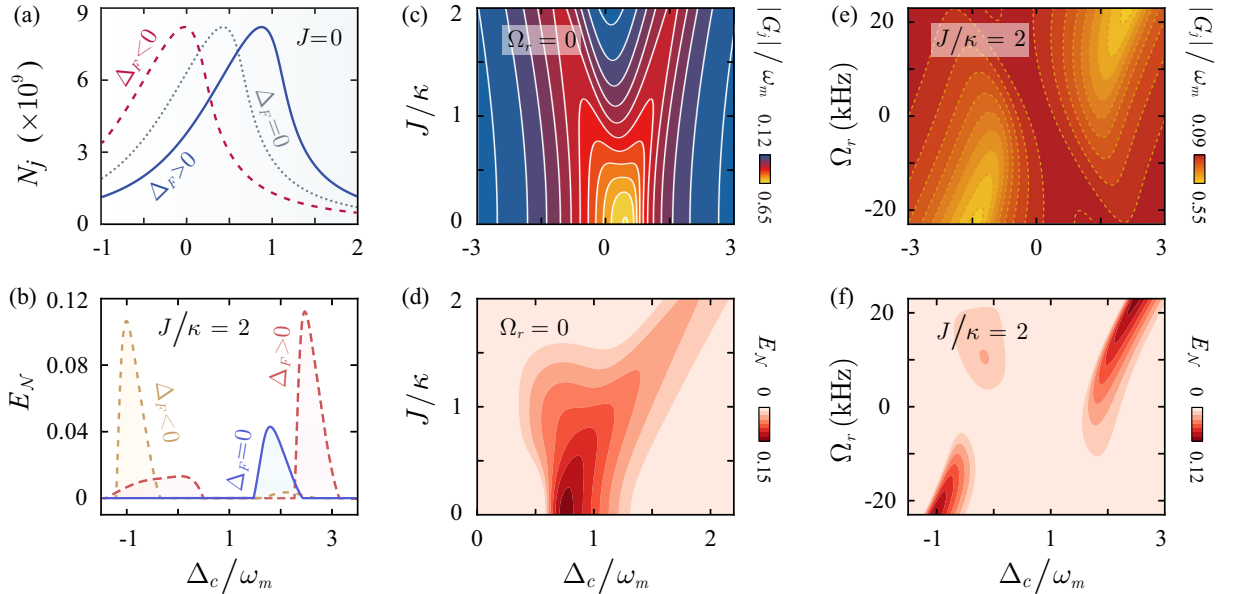


**Figure S3:** (a) Intracavity photon number for varying the scaled optical detuning  $\Delta_c/\omega_m$  from different driving directions. For nonspinning case, the counter-propagating modes are symmetric, however, classical isolation of light can emerge via mechanical rotation. (b) The logarithmic negativity  $E_N$  versus the scaled optical detuning  $\Delta_c/\omega_m$  in the case of  $J/\kappa = 2$ . Quantum nonreciprocity exists even in the presence of backscattering losses. (c) The effective COM coupling rate  $|G_j|$  and (d) the logarithmic negativity  $E_N$  as a function of the optical detuning  $\Delta_c/\omega_m$  and the optical coupling strength  $J/\kappa$  in a stationary resonator. (e) Plots of the effective COM coupling rate  $|G_j|$  and (f) the logarithmic negativity  $E_N$  as a function of the optical detuning  $\Delta_c/\omega_m$  and the spinning frequency  $\Omega_r$  in the case of  $J/\kappa = 2$ . We set  $\Omega = 8$  kHz in (a) and 23 kHz in (b). Other parameters are listed in Table I.

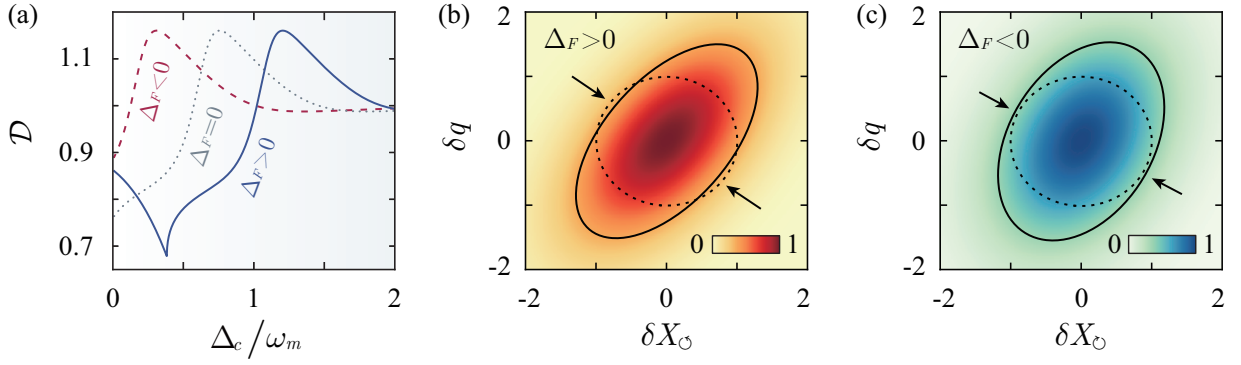


**Figure S4: Nonreciprocal entanglement dimensionality and two-mode squeezing in ideal resonators.** (a) Entanglement dimensionality versus the scaled optical detuning  $\Delta_c/\omega_m$  for different driving directions. (b-c) Projections of the measured reconstructed Wigner function compared with the ideal vacuum state at  $\Delta_c/\omega_m = 1.2$ , in which ellipses and circles indicate a drop by  $1/e$  of their respective maximum value. The input power is chosen as  $P = 100$  mW in (b) and (c). Other parameters are listed in Table I.

numbers. However, the nonreciprocal COM entanglement, characterizing different quantum correlations between the optical field and the mechanical mode, is a truly quantum phenomenon and fundamentally different from the classical nonreciprocity.

In experimental fabrications, inherent non-ideality such as surface roughness or material inhomogeneity, is inevitable and always leads to backscattering of photons. When the counter-propagating modes are near resonant and the driving field is intensive, backscattering can lead to a coherent build-up of the reflected mode even if the individual reflections are very weak, then resulting in the coupling of the counter-propagating modes [S10]. The backscattering process is usually harmful to the observation of quantum effects. However, we have demonstrated that the nonreciprocal control could provide a feasible way to overcome such nonideal effects [see Figs. S3(b)]. Here, to further present the relationship between the backscattering process and the nonreciprocal control, we plot the effective COM coupling rates  $|G_j|$  and the logarithmic negativity  $E_{\mathcal{N}}$  versus the optical detuning  $\Delta_c$  and the rotation speed  $\Omega_r$  in Figs. S3(c) - S3(f). For the nonspinning case, as shown in Figs. S3(c) - S3(d), the effective COM coupling rate of the driving mode decreases due to the excitation of the reflected mode, thus leading to the suppression of COM entanglement. However, in the presence of rotation, the resonance frequency of the counter-propagating modes can be freely tuned by adjusting the Sagnac-Fizeau frequency shift. In this case, the CW and CCW modes can be perfectly isolated, and thereby preventing the build-up of the reflected mode caused by the backscattering process. As a result, for practical devices with inherent non-ideality, it can be fully immune to backscattering process via suitable nonreciprocal control and thus becomes an ideal platform for manipulating quantum effect such COM entanglement [see Figs. S3(e) and S3(f)].

#### S4. ENTANGLEMENT DIMENSIONALITY AND TWO MODE SQUEEZING

Accompanied with nonreciprocal COM entanglement, our proposed scheme also shows the potential to realize other quantum nonreciprocity. For example, the entanglement dimensionality, characterizing the number of independent degrees of freedom of entangled subsystems, can possess similar properties to the logarithmic negativity in spinning resonators. For general two-mode Gaussian state, the entanglement dimensionality is defined as [S11]:

$$\mathcal{D} = 1/(2\nu^-), \quad (\text{S4.20})$$

where  $\nu^-$  is the lowest symplectic eigenvalue of the partial transpose of the selected bipartite  $4 \times 4$  correlation matrix  $\mathcal{V}_{bp}$ . As shown in Fig. S4(a), the dimensionality  $\mathcal{D}$  remains the same independently of driving directions for stationary case. However, in the presence of rotation, it can be remarkably different by reversing the driving directions, indicating the achievement of nonreciprocal entanglement dimensionality.

Besides, unidirectional cross-quadrature two-mode squeezing is also achievable in the spinning resonators. Specifically, the degrees of two-mode squeezing can be well visualized by the quasiprobability Wigner function. Since the system finally evolves into Gaussian state, the Wigner function can be written as a multivariate normal distribution [S12]:

$$W(\psi) = \frac{\exp\left[-\frac{1}{2}\left(\psi\mathcal{V}_{bp}^{-1}\psi^\dagger\right)\right]}{\pi^2\sqrt{\det\mathcal{V}_{bp}}}, \quad (\text{S4.21})$$

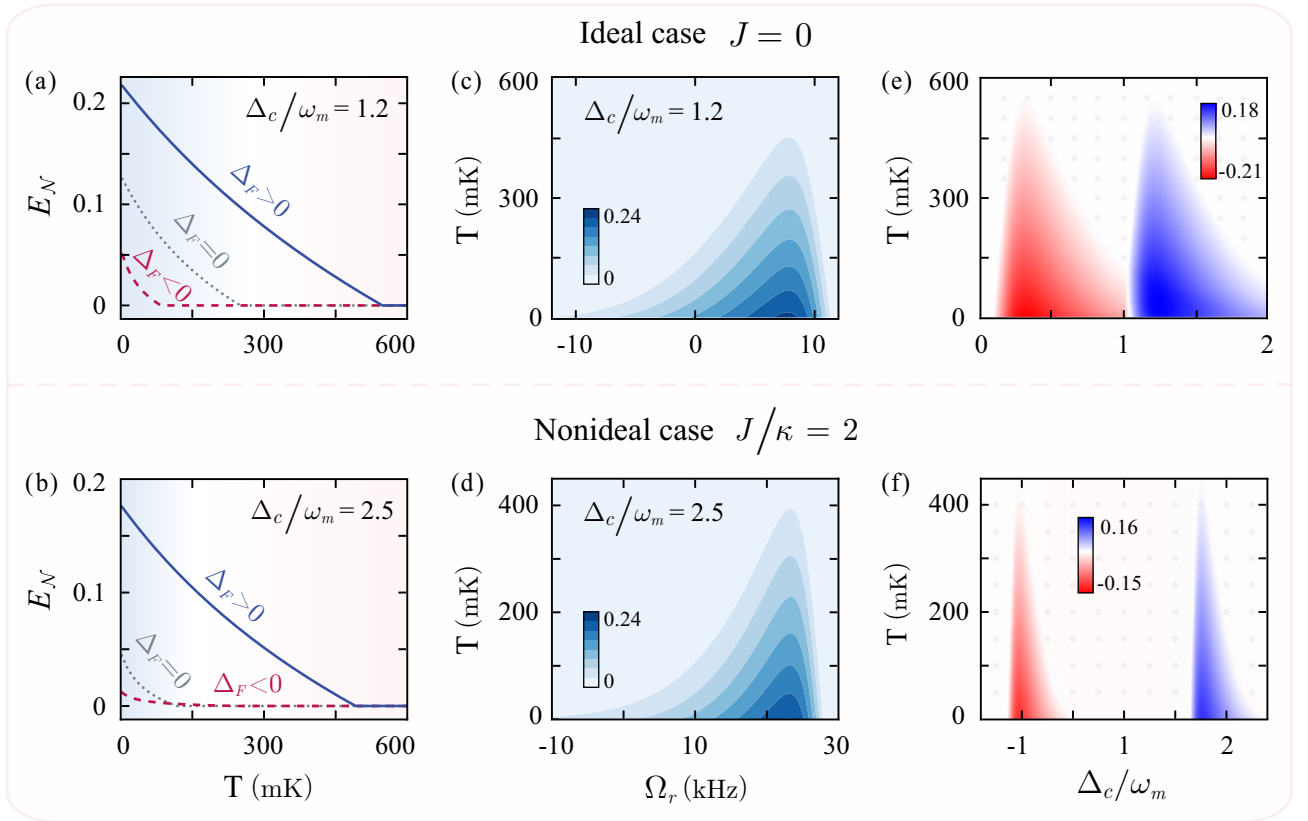


**Figure S5: Thermal effect on nonreciprocal COM entanglement.** (a-b) The logarithmic negativity  $E_{\mathcal{N}}$  as a function of the environment temperature  $T$  for different driving directions. (c-d) Density plots of the logarithmic negativity  $E_{\mathcal{N}}$  versus the angular velocity  $\Omega_r$  and the environment temperature  $T$ . (e-f) The entanglement difference between the counter-propagating modes,  $\Delta E_{\mathcal{N}}$ , versus the scaled optical detuning  $\Delta_c/\omega_m$  and the environment temperature  $T$ . We fix the rotation speed at  $\Omega = 8$  kHz in (a) and (e), and  $\Omega = 23$  kHz in (b) and (f). Other parameters are listed in Table I.

where  $\psi = (\delta q, \delta p, \delta X_j, \delta Y_j)$  is the state vector of the selected quadrature fluctuations corresponding to  $\mathcal{V}_{bp}$ . Figures S4(b) and S4(c) show the characteristic projections of the reconstructed Wigner function  $W(\psi)$  of the measured covariance matrix  $\mathcal{V}_{bp}$  compared with the theoretical vacuum state  $V_{\text{vac}} = I/2$  ( $I$  is the identity matrix). In the case of  $\Delta_F > 0$ , the  $\{\delta q, \delta X_{\odot}\}$  projection of  $W(\psi)$  is below standard quantum limit in the diagonal directions, that is, achieving cross-quadrature squeezing between CCW optical mode and mechanical mode. In contrast, when driving direction is reversed, such kind of cross-quadrature squeezing disappears between CW optical mode and mechanical mode, which is a clear signature of achieving quantum nonreciprocity in cross-quadrature squeezing.

These results as revealed here may provide a promising new way for the realization of chiral quantum information processing or quantum networks [S13–S15].

## S5. INFLUENCE OF THERMAL EFFECT ON OPTOMECHANICAL ENTANGLEMENT

As it is well known, quantum effects are usually fragile to environment since thermal noises always tend to destroy quantum correlations. Therefore, protecting quantum resources from environmental thermal excitations is essential for achieving quantum nonreciprocity. To more clearly see the influence of the thermal effect on COM entanglement, we plot the logarithmic negativity  $E_{\mathcal{N}}$  with respect to the environment temperature  $T$  in Figs. S5(a)–S5(d). Specifically, it is found that nonreciprocal COM entanglement in a selected direction can exist at comparatively high temperature compared to the stationary case. Moreover, for devices with suitable rotation speed, the robustness of COM entanglement to thermal noises can be further improved. In addition, by defining the difference of COM entanglement between the counter-propagating modes:  $\Delta E_{\mathcal{N}} \equiv E_{\mathcal{N},\odot} - E_{\mathcal{N},\ominus}$ , we demonstrate the dependence of quantum nonreciprocity on environmental temperature in Figs. S5(e) and S5(f). It is seen that the condition  $\Delta E_{\mathcal{N}} \neq 0$  can still be satisfied even at  $T \sim 600$  mK.

## S6. SYSTEM PARAMETERS

In Table I we collect the main symbols and parameters which have been used in this work.

Symbol	Definition	Name	Value
$\omega_m$		Mechanical resonance frequency	63 MHz
$\gamma_m$		Mechanical linewidth	5.2 kHz
$Q_m$	$\omega_m/\gamma_m$	Mechanical quality factor	$1.21 \times 10^4$
T		Mechanical bath temperature	130 mK
$n_m$	$[\exp(\hbar\omega_m/k_B T) - 1]^{-1}$	Thermal phonon occupation	269.4
$m$		Effective mass	10 ng
$x_{zP}$	$\sqrt{\hbar/(m\omega_m)}$	Zero point fluctuations	0.41 fm
$\omega_c$		Optical resonance frequency	1.22 PHz
$\lambda$		Laser wavelength	1.55 $\mu\text{m}$
$\kappa$		Cavity linewidth	38.0 MHz
$Q$	$\omega_c/\kappa$	Optical quality factor	$3.2 \times 10^7$
$P$		input laser power	20 mW or 100 mW
$G_0$		Single-photon optomechanical coupling rate	452.1 Hz
$C_0$	$4G_0^2/(\kappa\gamma_m)$	Single-photon optomechanical cooperativity	$4.14 \times 10^{-6}$
$R$		Sphere radius	1.1 mm
$r$		Fiber radius	544 nm
$\Omega$		Spinning frequency	8 kHz or 23 kHz
E		Young modulus of silica	75 GPa
$\Upsilon$		Elastic limit of silica	9 GPa
$\varepsilon_0$		Dielectric constant of air	1
$\varepsilon_1$ ( $\varepsilon_2$ )		Dielectric constant of silica	3.9
$n_0$		Refractive index of air	1
$n_1$ ( $n_2$ )		Refractive index of silica	1.48

TABLE I: Feasible parameters. Unless specified otherwise, these parameters apply to all evaluations in the text.

\* Electronic address: [lmkuang@hunnu.edu.cn](mailto:lmkuang@hunnu.edu.cn)

† Electronic address: [jinghui73@gmail.com](mailto:jinghui73@gmail.com)

- [S1] S. Maayani, R. Dahan, Y. Kligerman, E. Moses, A. U. Hassan, H. Jing, F. Nori, D. N. Christodoulides, and T. Carmon, Flying couplers above spinning resonators generate irreversible refraction, *Nature (London)* **558**, 569 (2018).
- [S2] R. Reimann, M. Doderer, E. Hebestreit, R. Diehl, M. Frimmer, D. Windey, F. Tebbenjohanns, and L. Novotny, GHz Rotation of an Optically Trapped Nanoparticle in Vacuum, *Phys. Rev. Lett.* **121**, 033602 (2018).
- [S3] J. Ahn, Z. Xu, J. Bang, Y.-H. Deng, T. M. Hoang, Q. Han, R.-M. Ma, and T. Li, Optically Levitated Nanodumbbell Torsion Balance and GHz Nanomechanical Rotor, *Phys. Rev. Lett.* **121**, 033603 (2018).
- [S4] Y. Bellouard, A. A. Said, and P. Bado, *Opt. Express* **13**, 6635 (2005).
- [S5] J. Chen, G. Zhou, L. Zhang, and W. Sun, Influence of Intermolecular Force on the Head-Disk Interface of HDD with High Recording Density, in *2009 Symposium on Photonics and Optoelectronics* (IEEE, 2009) pp. 1–4.
- [S6] L. Wu and D. B. Bogy, Effect of the Intermolecular Forces on the Flying Attitude of Sub-5 NM Flying Height Air Bearing Sliders in Hard Disk Drives, *J. Tribol.* **124**, 562 (2002).
- [S7] R. Joyce, H. Sterling, and J. Alexander, Silicon oxide and nitride films deposited by an r.f. glow-discharge, *Thin Solid Films* **1**, 481 (1968).

- [S8] H. Sugiura, R. Ikeda, K. Kondo, and T. Yamadaya, Densified silica glass after shock compression, *J. Appl. Phys.* **81**, 1651 (1997).
- [S9] E. X. DeJesus and C. Kaufman, Routh-Hurwitz criterion in the examination of eigenvalues of a system of nonlinear ordinary differential equations, *Phys. Rev. A* **35**, 5288 (1987).
- [S10] A. Li, T. Van Vaerenbergh, P. De Heyn, P. Bienstman, and W. Bogaerts, Backscattering in silicon microring resonators: a quantitative analysis, *Laser Photon. Rev.* **10**, 420 (2016).
- [S11] C. Eltschka and J. Siewert, Negativity as an Estimator of Entanglement Dimension, *Phys. Rev. Lett.* **111**, 100503 (2013).
- [S12] G. Adesso, A. Serafini, and F. Illuminati, Extremal entanglement and mixedness in continuous variable systems, *Phys. Rev. A* **70**, 022318 (2004).
- [S13] P. Lodahl, S. Mahmoodian, S. Stobbe, A. Rauschenbeutel, P. Schneeweiss, J. Volz, H. Pichler, and P. Zoller, Chiral quantum optics, *Nature (London)* **541**, 473 (2017).
- [S14] H. J. Kimble, The quantum internet, *Nature (London)* **453**, 1023 (2008).
- [S15] K. Stannigel, P. Komar, S. J. M. Habraken, S. D. Bennett, M. D. Lukin, P. Zoller, and P. Rabl, Optomechanical Quantum Information Processing with Photons and Phonons, *Phys. Rev. Lett.* **109**, 013603 (2012).